Accepted for publication by International Journal of Non-Linear Mechanics on 17 July 2020

Design, Analysis and Experimental Validation of High Static and Low Dynamic Stiffness Mounts Based on Target Force Curves

Yu Sun[a,b], Jinsong Zhou[b,1], David Thompson[c], Tianchen Yuan[d], Dao Gong[b], Taiwen You[b]

[a] *Postdoctoral Station of Mechanical Engineering, Tongji University, Shanghai 201804, PR China*
[b] *Institute of Rail Transit, Tongji University, Shanghai 201804, PR China*
[c] *Institute of Sound and Vibration Research, University of Southampton, Southampton SO17 1BJ, UK*
[d] *School of Urban Railway Transportation, Shanghai University of Engineering Science, Shanghai 201620, PR China*

Abstract: In order to improve vibration isolation, soft components can be used in engineering applications, but this can lead to excessive static deflection. An ideal vibration isolator should have a high static stiffness to ensure that it has sufficient load carrying capacity; at the same time, it should have a low dynamic stiffness to maximize the vibration isolation frequency range. Recently, high static and low dynamic stiffness (HSLDS) mounts have been increasingly shown to have significant benefits for various engineering applications. This paper proposes a method for designing HSLDS mounts based on target force curves. In the design method, the HSLDS mount is obtained by placing a negative stiffness structure in parallel with a positive stiffness linear spring. The negative stiffness structure is achieved by using a roller-slider curve which can be designed according to the requirements to achieve the target force curve. HSLDS mounts are proposed with *n*th-order stiffness behaviour which are designed using the method presented here. The results show that, compared with lower order HSLDS mounts based on the same static stiffness, higher order HSLDS mounts have lower dynamic stiffness near the equilibrium position. The Average Method is used to analyze the dynamics of a system based on the *n*th-order HSLDS mounts, and the displacement transmissibility under harmonic excitation is obtained. The effects of different parameters on the transmissibility are studied. The results show that appropriately increasing the damping ratio is beneficial for the isolation performance of the HSLDS mount. Finally, an experimental prototype is designed and manufactured. The proposed design method and the vibration isolation performance of the HSLDS mount are verified by constant-frequency excitation experiments.

Key words: Target Force Curve; High Static and Low Dynamic Stiffness; Nonlinear Transfer Function; Vibration Reduction; Experimental Verification

1 Introduction

Vibration has a negative impact in many industrial applications. Consequently, vibration control technology is widely used in engineering fields such as rail vehicle systems[1], automobiles[2],

* Corresponding author.
E-mail address: jinsong.zhou@tongji.edu.cn

tall buildings[3], precision instruments[4], etc. In general, vibration control technology can be achieved by either passive or active control methods. An important form of passive vibration control is based on vibration isolation components, such as rubber[5], coil springs[6], etc. In order to have load-carrying capacity, these components require sufficiently high static stiffness. As a result, their dynamic stiffness is also high, and the low-frequency vibration isolation performance is poor. Active control[7] can make up for the shortcomings of passive control in low-frequency vibration isolation, but it requires external energy, complex structures, high cost and additional maintenance, so it is not as widely used. Low-frequency vibration isolation technology has the potential to be widely used, especially in the field of transportation vehicles such as automobiles and rail vehicles. It is especially important to reduce the vibration in the frequency region of highest sensitivity of the human body, 4~8Hz[8].

In recent years, many researchers have proposed a passive vibration isolation technology based on high static and low dynamic stiffness (HSLDS) vibration isolation mounts[9] which can achieve low frequency vibration isolation performance, while retaining sufficient load-carrying capacity. This idea was first proposed more than 30 years ago under the name quasi-zero stiffness (QZS)[10]. Several different forms of HSLDS structures are introduced, for example, in Ref. [11, 12]. Due to the complex requirements of HSLDS vibration isolation mounts, it is difficult to obtain a desirable mechanical characteristic based on a single component; instead it usually requires a combination of several components. Many forms of HSLDS mount structure have been proposed, the key to which is to find a mechanism that provides a negative stiffness. By connecting a negative stiffness structure in parallel with a positive stiffness spring, a mount can be obtained with high static stiffness and low dynamic stiffness near the equilibrium position. According to the form of negative stiffness structure, HSLDS mounts can be achieved by using three parallel springs, buckling Euler rods, disc springs, magnetic components, or cam–roller–spring, etc.

Carrella et al. [13, 14] discussed the static force characteristic of HSLDS mounts based on three parallel springs. By deriving an optimal set of parameter values, the mount can be designed to be a QZS mechanism. In Ref. [15] they investigated the force and displacement transmissibility of such types of HSLDS mount. Le and Ahn[16] proposed a negative stiffness structure which consists of two horizontal springs and two bars to provide negative stiffness in the vertical direction. This type of HSLDS mount was extended by including a mechanism that enables easy and quick adjustment of the parameters of the configuration[17].

Liu et al. [18] presented a HSLDS mount by connecting Euler buckled beams with a linear spring. The theoretical dynamic properties were investigated by using the Harmonic Balance Method. The effects of parameter imperfections were discussed in Ref. [19] and an experimental study was presented in Ref. [20].

Meng et al.[21, 22] presented a QZS isolator by combining a disc spring with a vertical linear spring. A parameter optimization was adopted to achieve a wide displacement range around the equilibrium position. The force, absolute displacement, and acceleration transmissibility of the QZS isolator were defined and analyzed. In Refs. [23, 24], Valeev et al. made a compact disc QZS isolator using elastic material. Their experimental study showed that the natural frequency of the developed isolator was less than 1 Hz.

In magnetic HSLDS mounts, the negative stiffness can be obtained by arranging three cuboidal magnets configured in repulsive interaction [25]. To improve the effective frequency range, Ref. [26] presented a HSLDS mount by using linear mechanical springs and magnets, in which a permanent

magnet was arranged at the outer edge of each spring. Dong et al.[27] proposed a magnetic HSLDS mount by combining a magnetic negative stiffness spring and a spiral flexural spring in parallel, in which the negative spring comprised three magnetic rings configured in attraction.

Zhou et al.[28] presented a QZS vibration isolation system by using the conceptual design of cam–roller–spring mechanisms, the slideway of which is semi-circular. By replacing the slideway with a user-defined noncircular profile, Li et al [29] obtained a QZS isolator with pure-cubic restoring force. In fact, the restoring force of such a nonlinear isolator can be designed as any order, i.e. 2, 3, 4, 5 etc.

Although the HSLDS vibration isolation system has been proposed 30 years ago, it has seen increased interest in recent years. Most of the relevant research papers discuss theoretical developments and laboratory experiments, and few studies are conducted in conjunction with specific engineering applications. To extend these previous studies, this paper proposes and analyzes a unified method for designing HSLDS mounts based on a cam–roller–spring mechanism with an arbitrary target force curve which is then applied by way of example to *n*th-order polynomial stiffness functions and an experimental prototype is built. The rest of this paper is organized as follows: In Section 2, the design method of HSLDS mounts with different nonlinear stiffness orders is presented based on target force curves. The *n*th-order HSLDS mounts with both odd and even orders are defined, designed and static force analysis is applied. In Section 3, the harmonic response, and displacement transmissibility of each order of HSLDS mounts are solved by the Average Method[30]. The effects of various parameters on the transmissibility of HSLDS mounts are analyzed. In Section 4, an experimental prototype is designed and manufactured. The proposed design method and the low-frequency vibration isolation performance of the HSLDS mount are verified by constant-frequency excitation experiments. Conclusions are summarized in Section 5.

2 Design method

The proposed isolator is shown schematically in Fig. 1. It consists of a roller guide support, two lateral springs, two rollers, a vertical spring, and a height adjuster. The isolator supports an isolated object. The roller guide support, lateral springs, and rollers constitute a negative stiffness structure that produces a negative stiffness in the vertical direction. The negative stiffness structure is connected in parallel with a vertical spring which provides positive stiffness. The vertical dynamic stiffness of the HSLDS mount is given by the sum of the dynamic stiffness of the negative stiffness structure and the vertical spring. The curved surfaces of the roller guide support can be designed based on the target force-deflection curve. When the isolated object is placed in equilibrium on the HSLDS mount, it can be arranged that the midpoint of the curved surface is in contact with the roller by the action of the height adjuster.

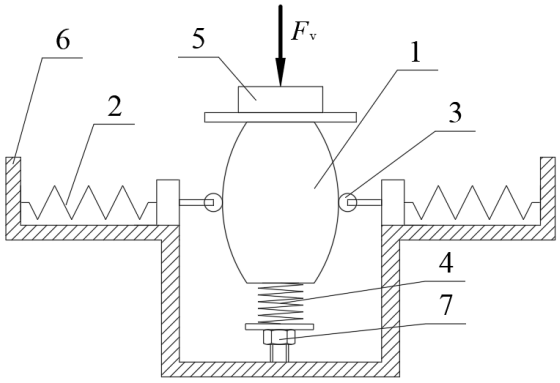

Fig. 1. Schematic design of the HSLDS mount based on target force curve (1-roller guide support, 2- lateral spring, 3-roller, 4-vertical spring, 5- isolated object, 6-fitting seat, 7-height adjuster)

The left and right guides are assumed to be symmetrical, and the force analysis of the left guide is used as an example, as shown as Fig. 2. This produces a negative stiffness in the vertical direction when the roller guide surface is convex, as shown in Fig. 2(a). In this case, when the isolated object moves upwards, the vertical component of the force exerted by the rollers is also upward, which corresponds to a negative stiffness.

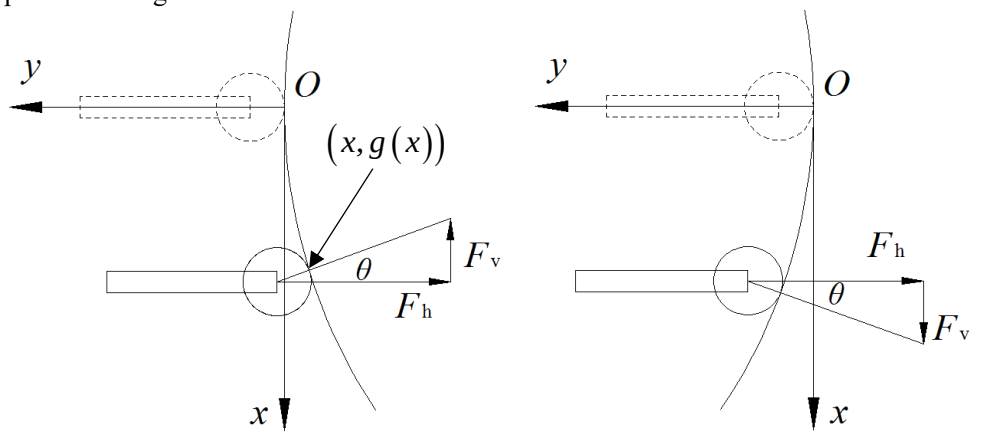

(a) Force schematic (convex) (b) Force schematic (concave)

Fig. 2. Force schematic of the HSLDS mount

The shape of the guide surface is defined by the function $y=g(x)$. It can be assumed that the effect of the roller radius on the system is negligible. As shown in Fig. 2(a), the contact point is (x, $g(x)$) when the deflection of the isolated object from the equilibrium position is x (g is negative in Fig. 2(a)). The gradient at the contact point is $g'(x)$, which is equal to tanθ. The spring deformation can be expressed as $\Delta l + g(x)$, where Δl is the initial pre-deformation of the lateral springs. Based on the force analysis, the force of the mount in the vertical direction can be expressed as

$$f(x) = k_v x + k_h (\Delta l + g(x)) g'(x) \tag{1}$$

where $g'(x)=\dfrac{\mathrm{d}g}{\mathrm{d}x}$, k_v is the stiffness of the vertical spring, $k_h/2$ is the stiffness of the lateral spring for one side. Rearranging Eq. (1) gives

$$f(x)\mathrm{d}x = k_h \Delta l \mathrm{d}g(x) + k_h g(x)\mathrm{d}g(x) + k_v x\mathrm{d}x \tag{2}$$

By integrating both sides one can obtain

$$\int f(x)\mathrm{d}x = k_h \Delta l g(x) + \frac{1}{2}k_h g(x)^2 + \frac{1}{2}k_v x^2 + C \tag{3}$$

where C is a constant. According to the desired equilibrium condition, the boundary conditions of

Eq. (3) are $f(0) = g(0) = 0$ and hence $C = 0$. For a specific target force curve, the corresponding roller slide curve can be obtained by numerical calculation. Eq. (3) can be regarded as a quadratic polynomial equation in $g(x)$, and the solution can be obtained as

$$g(x)=-\Delta l+\sqrt{\Delta l^2-\left(\frac{k_v}{k_h}x^2-\frac{2}{k_h}\int f(x)dx\right)} \tag{4}$$

It can be verified that the same result can be acquired according to force analysis of Fig. 2(b). When $f(x)$ represents a linear system (e.g. $f(x)=k_v x$), it can be verified that $g(x)=0$, and the forces exhibited by the lateral springs counteract each other, resulting in no net vertical force provided by the lateral springs.

To verify the validity of the design method, two design examples are presented. Example 1 is a third order HSLDS mount, the force expression of which is

$$f(x)=ak_v x^3 \tag{5}$$

So,

$$\int f(x)\mathrm{d}x=\int ak_v x^3\mathrm{d}x=\frac{1}{4}ak_v x^4 \tag{6}$$

Then, $g(x)$ can be obtained as

$$g(x)=-\Delta l+\sqrt{\Delta l^2-\frac{k_v}{k_h}\left(x^2-\frac{a}{2}x^4\right)} \tag{7}$$

Taking a=1 m^{-2}, $k_v=10^5$ N/m, $k_h=2\times10^5$ N/m, Δl=0.8 m, the roller guide curve can be acquired based on Eq.(7) and the force-displacement curve and the roller guide curve are obtained as shown Fig. 3(a) and (b).

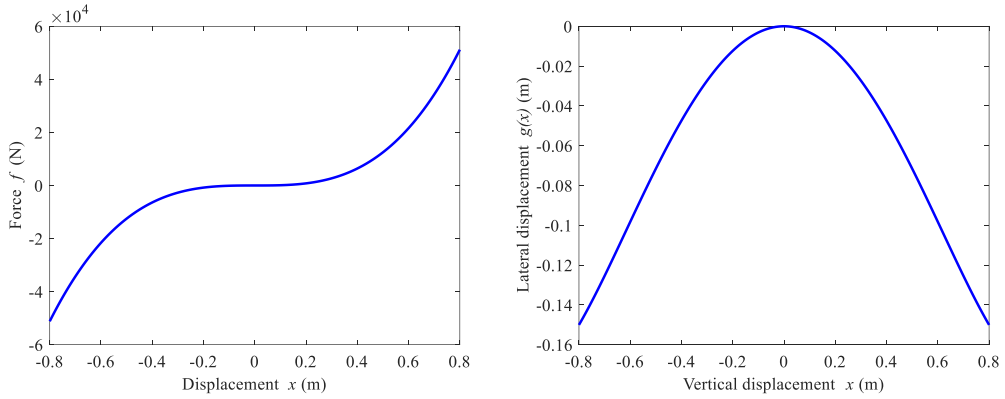

(a) (b)

Fig. 3. Example 1 (a) The target force-displacement curve $f(x)$; (b) The roller guide curve $g(x)$.

The target force curve of Example 2 is a piecewise function, which is expressed as

$$f(x)=\begin{cases} ak_v\left((x+0.4)^3-2\cdot0.2^3\right) & -0.6\le x\le -0.2 \\ ak_v x^3 & -0.2<x<0.2 \\ ak_v\left((x-0.4)^3+2\cdot0.2^3\right) & 0.2\le x\le 0.6 \end{cases} \tag{8}$$

By assuming the same parameter values, the force characteristic of the target force curve is as shown in Fig. 4(a). In the figure, different line styles represent different segments of Eq.(8). The resulting roller guide curve $g(x)$ is shown as Fig. 4(b).

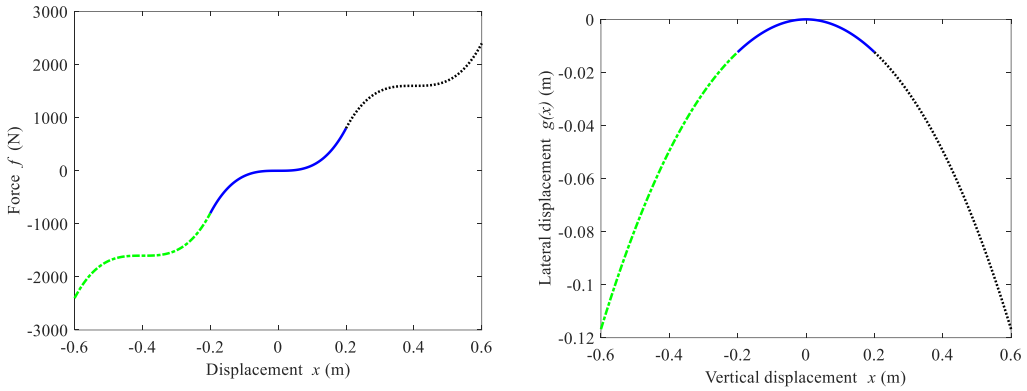

(a) (b)

Fig. 4. Example 2 (a) The target force curve $f(x)$; (b) The roller guide curve $g(x)$.

From the above two examples it can be seen that the proposed method allows a specific mount to be designed based on a target force curve. By designing the shape of the slider curve as shown in Fig. 1, the target force curve is achieved in the vertical direction. However, the stiffness curve cannot be modified once the component design is complete. Therefore, the proposed component design method is suitable for the case where the weight of the vibration-isolated object is constant.

3 Analysis of *n*th-order HSLDS mounts

3.1 *Definition of nth-order HSLDS mounts*

The target force expression of an *n*th-order HSLDS mount is given by

$$f_n(x)=ak_e x|x|^{n-1} \tag{9}$$

where k_e is the stiffness of the equivalent linear system which is defined below, a is a parameter related to the static deflection, n=1,2,3… By differentiating Eq. (9), the stiffness of the *n*th-order HSLDS mounts can be obtained as

$$k_n = ank_e|x|^{n-1} \tag{10}$$

An equivalent linear system is defined as a system with the same static deflection x_s under a given static load f_0 as the *n*th-order HSLDS mount. If the vertical stiffness of the equivalent linear system is $k_e = f_0/x_s$, the parameter a in Eq. (10) can be determined as

$$a = x_s^{-(n-1)} \tag{11}$$

The force and stiffness of the *n*th-order HSLDS mounts are shown for an example case with x_s=0.1 m, k_e=10^5 N/m in Fig. 5(a) and (b), respectively. An equivalent linear system with stiffness k_e=10^5 N/m is added to the figure for comparison. Relative to the equilibrium position x=0, when the displacement is $-x_s$ = –0.1 m, the static load f_0 = 10^4 N has been removed in each case. It can be seen from Fig. 5(b) that the stiffness of each HSLDS curve near the equilibrium position is close to 0. The restoring force of the higher-order HSLDS mounts near the equilibrium position is smaller than that of the lower-order ones for the same displacement. This indicates that, compared with lower order HSLDS mounts based on the same static stiffness, higher-order HSLDS mounts have a lower dynamic stiffness and larger stroke length. Compared with the 2nd-order HSLDS mount, when the force varies between ±0.1f_0, for example, the stroke length of the 5th-order HSLDS mount is twice as large as that of the 2nd-order one.

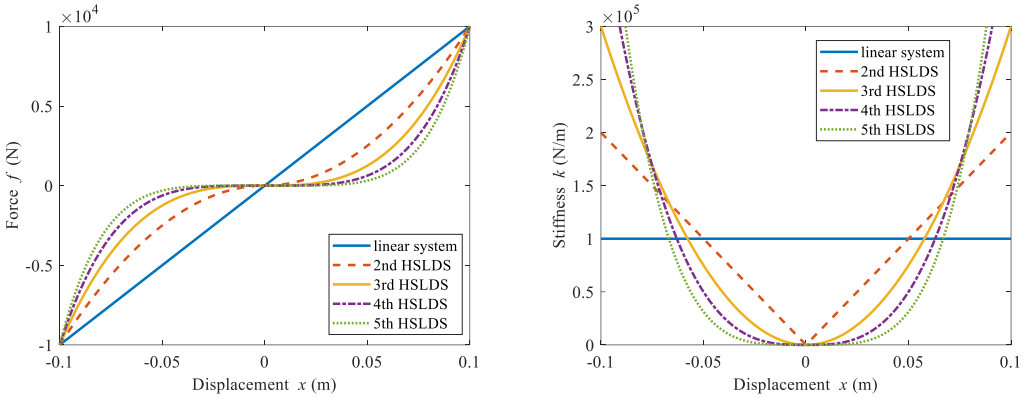

(a) (b)

Fig. 5. (a) Force-displacement curve of *n*th-order HSLDS mounts; (b) Stiffness-displacement curve of *n*th-order HSLDS mounts.

Allowing for the boundary conditions at x=0, and the presence of the stiffness k_v, the roller guide curves of the *n*th-order HSLDS mounts can be obtained according to Eq. (4), which can be expressed as

$$g_n(x) = -\Delta l + \sqrt{\Delta l^2 - \left(\frac{k_v}{k_h} x^2 - \frac{2ak_e}{(n+1)k_h} |x|^{n+1} \right)} \tag{12}$$

The roller guide curves of the *n*th-order HSLDS mounts obtained according to Eq. (12) for x_s=0.1 m, k_e=10^5 N/m, Δl=0.08 m, k_v=10^5 N/m, and k_h=2×10^5 N/m are shown in Fig. 6, in which the equivalent linear system is added for comparison. Note that, here, k_e and k_v are equal but in the general case they do not need to be. The static deflections of the *n*th-order HSLDS mounts shown in the figure are the same, which are decided by Eq. (9) and Eq. (11). The static deflection is mg/k_e when the system carries a vibration-isolated object with a weight of mg; that is to say the static property is determined by the stiffness of the equivalent linear system. As described above, the roller guide curve of the equivalent linear system is a straight line. It can be seen from the figure that as the order of the HSLDS mount increases, the required lateral displacement of the roller guide curve increases. Taking the vertical displacement of 0.08 m as an example, the lateral displacement of the 3rd-order HSLDS mount is smaller than that of the 5th-order one by 24%.

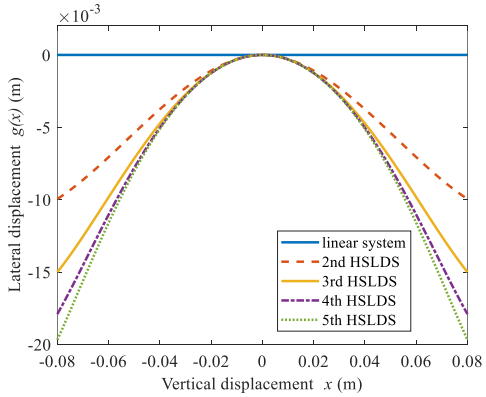

Fig. 6. The roller guide curve of the *n*th-order HSLDS mounts.

3.2 *Dynamic analysis of nth-order HSLDS mounts*

For the case of a supported mass m, and including viscous damping and a harmonic displacement excitation $z_e = Z_e \cos(\omega t)$ of the base, the equation of motion of the mass is given by

$$m\ddot{z} + c\dot{z} + ak_e z|z|^{n-1} = m\omega^2 Z_e \cos(\omega t) \tag{13}$$

where $z = x - z_e$ is the relative displacement between the isolated object and the base. To solve the equation, the following non-dimensional variables are introduced: $x_s = mg/k_e$, $\hat{x} = x/x_s$, $\hat{z}_e = z_e/x_s$, $\hat{z} = z/x_s$, $\hat{Z} = Z/x_s$, $\hat{Z}_e = Z_e/x_s$, $\omega_0 = \sqrt{k_e/m}$, $\Omega = \omega/\omega_0$, $\tau = \omega_0 t$, $\zeta = c/(2m\omega_0)$. Using Eq. (11), Eq. (13) can be converted into a dimensionless equation as

$$\hat{z}'' + 2\zeta\hat{z}' + \hat{z}\left|\hat{z}\right|^{n-1} = \Omega^2 \hat{Z}_e \cos(\Omega\tau) \tag{14}$$

By assuming a steady-state response of the form $\hat{z} = \hat{Z}\cos(\Omega\tau + \varphi)$, and applying the Average Method, the steady-state response of the system can be expressed as

$$\hat{z} = \hat{Z}\cos(\Omega\tau + \varphi) \tag{15}$$

$$\hat{z}' = -\Omega\hat{Z}\sin(\Omega\tau + \varphi) \tag{16}$$

where $\hat{Z}$ and φ are initially assumed to be functions of τ. Taking the derivative of Eq. (15) and (16) gives

$$\hat{z}' = \hat{Z}'\cos(\Omega\tau + \varphi) - \hat{Z}\sin(\Omega\tau + \varphi)\cdot(\Omega + \varphi') \tag{17}$$

$$\hat{z}'' = -\Omega\hat{Z}'\sin(\Omega\tau + \varphi) - \Omega\hat{Z}\cos(\Omega\tau + \varphi)\cdot(\Omega + \varphi') \tag{18}$$

So,

$$\hat{Z}'\cos(\Omega\tau + \varphi) - \hat{Z}\sin(\Omega\tau + \varphi)\varphi' = 0 \tag{19}$$

Substituting Eq. (15), (16), and (19) into Eq. (14) gives

$$-\Omega\hat{Z}'\sin(\Omega\tau + \varphi) - \varphi'\Omega\hat{Z}\cos(\Omega\tau + \varphi) = \mathrm{H} \tag{20}$$

where

$$\begin{aligned}\mathrm{H} = {} & \Omega^2\hat{Z}\cos(\Omega\tau + \varphi) + 2\zeta\Omega\hat{Z}\sin(\Omega\tau + \varphi) \\ & - \hat{Z}^n\cos(\Omega\tau + \varphi)\left|\cos(\Omega\tau + \varphi)\right|^{n-1} + \Omega^2\hat{Z}_e\cos(\Omega\tau)\end{aligned} \tag{21}$$

By combining Eq. (19) and (20), the following can be obtained

$$\hat{Z}' = -\frac{\mathrm{H}}{\Omega}\sin(\Omega\tau + \varphi) \tag{22}$$

$$\varphi' = -\frac{\mathrm{H}}{\hat{Z}\Omega}\cos(\Omega\tau + \varphi) \tag{23}$$

By replacing the above equations with the mean value in one period, and considering that it remains constant for one period of ($\Omega\tau + \varphi$), the average equation can be obtained as

$$\hat{Z}' = -\frac{\Omega}{2\pi}\int_0^{\frac{2\pi}{\Omega}}\frac{\mathrm{H}}{\Omega}\sin(\Omega\tau + \varphi)d\tau \tag{24}$$

$$\varphi' = -\frac{\Omega}{2\pi}\int_0^{\frac{2\pi}{\Omega}}\frac{\mathrm{H}}{\hat{Z}\Omega}\cos(\Omega\tau + \varphi)d\tau \tag{25}$$

So, Eq. (24) and (25) can be simplified as

$$\hat{Z}' = -\frac{\Omega\hat{Z}_e\sin\varphi}{2} - \zeta\hat{Z} \tag{26}$$

$$\varphi' = -\frac{\Omega \hat{Z}_e \cos\varphi}{2\hat{Z}} - \frac{\Omega}{2} + \frac{\hat{Z}^{n-1}}{2\pi\Omega}\int_0^{2\pi}\left|\cos^{n+1}(\tau)\right| d\tau \tag{27}$$

By setting $\hat{Z}'=0$ and $\varphi'=0$, the amplitude-frequency response function of the *n*th-order HSLDS mounts can be expressed as

$$\left(\hat{Z}^2 - \hat{Z}_e{}^2\right)\Omega^4 + \left(4\zeta^2\hat{Z}^2 - \hat{Z}^{n+1}\int_0^{2\pi}\frac{2}{\pi}\left|\cos^{n+1}(\tau)\right| d\tau\right)\Omega^2 + \left(\int_0^{2\pi}\frac{1}{\pi}\left|\cos^{n+1}(\tau)\right| d\tau\right)^2 \hat{Z}^{2n} = 0 \tag{28}$$

The above equation is a quadratic polynomial equation in Ω^2. Values of the non-dimensional frequency Ω can be obtained for a given value of $\hat{Z}$ as

$$\Omega_{1,2} = \sqrt{\frac{\hat{Z}^{n+1}\int_0^{2\pi}\frac{2}{\pi}\left|\cos^{n+1}(\tau)\right| d\tau - 4\zeta^2\hat{Z}^2 \pm \sqrt{16\zeta^4\hat{Z}^4 + \hat{Z}_e{}^2\hat{Z}^{2n}\left(\int_0^{2\pi}\frac{2}{\pi}\left|\cos^{n+1}(\tau)\right| d\tau\right)^2 - \zeta^2\hat{Z}^{n+3}\int_0^{2\pi}\frac{16}{\pi}\left|\cos^{n+1}(\tau)\right| d\tau}}{2\left(\hat{Z}^2 - \hat{Z}_e{}^2\right)}} \tag{29}$$

It can be verified that Eq. (29) is the solution of the linear system when *n* = 1. When *n* = 3, the solution of the 3rd-order HSLDS mount under harmonic displacement excitation can be obtained as

$$\Omega_{1,2} = \sqrt{\frac{3\hat{Z}^4 - 8\zeta^2\hat{Z}^2 \pm \hat{Z}^2\sqrt{64\zeta^4 + 9\hat{Z}_e{}^2\hat{Z}^2 - 48\zeta^2\hat{Z}^2}}{4\left(\hat{Z}^2 - \hat{Z}_e{}^2\right)}} \tag{30}$$

It can be verified that Eq. (30) is consistent with the results of Ref. [21] obtained by Harmonic Balance Method.

3.3 *Displacement transmissibility*

In order to obtain the displacement transmissibility of the *n*th-order HSLDS mounts, the dimensionless displacement of the isolated object is obtained as

$$\hat{x} = \hat{z} + \hat{z}_e = \hat{Z}\cos\left(\Omega\tau + \varphi\right) + \hat{Z}_e\cos\left(\Omega\tau\right) \tag{31}$$

So, the displacement transmissibility can be expressed as

$$T_D = \frac{|\hat{x}|}{|\hat{z}_e|} = \frac{\sqrt{\hat{Z}^2 + \hat{Z}_e{}^2 + 2\hat{Z}\hat{Z}_e\cos\left(\varphi\right)}}{\hat{Z}_e} \tag{32}$$

where $\cos\left(\varphi\right)$ can be obtained from Eq (27).

For linear systems, the displacement transmissibility is

$$T_l = \sqrt{\frac{1+(2\zeta\Omega)^2}{(1-\Omega^2)^2 + (2\zeta\Omega)^2}} \tag{33}$$

where Ω is the non-dimensional frequency given by the ratio of the excitation frequency to the natural frequency of the equivalent linear system. The displacement transmissibility of the *n*th-order HSLDS mounts obtained from Eq.(32), for ζ=0.1，$\hat{Z}_e$=0.1 and 0.5 is shown as Fig. 7(a) and (b). It can be seen from Fig. 7(a) that the maximum value of transmissibility for each HSLDS mount is lower than that of the equivalent linear system, and the corresponding peak frequency is also lower. Especially when the non-dimensional frequency is around 1, the displacement transmissibility of the HSLDS mounts is much lower than that of the equivalent linear system. Fig. 7(b) shows results for a higher excitation amplitude. Increasing the excitation amplitude increases the maximum value of the transmissibility, but the lower branches of the transmissibility of the HSLDS mounts are still

much lower than the equivalent linear system when the non-dimensional frequency is between about 1 and 10.

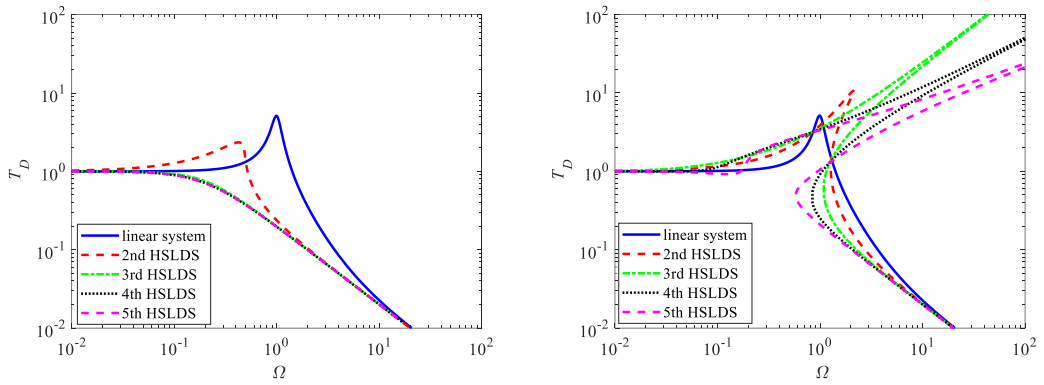

(a) (b)

Fig. 7. Displacement transmissibility of *n*th-order HSLDS mounts for (a) ζ=0.1, $\hat{Z}_e$=0.1; (b) ζ=0.1, $\hat{Z}_e$=0.5.

The effect of various parameters on the displacement transmissibility of the 3rd-order HSLDS mount is shown in Fig. 8 (a) and (b). Unless mentioned in the figures the values of the parameters are ζ=0.1, $\hat{Z}_e$=0.1. Fig. 8 (a) shows the effect of varying the damping ratio ζ on the displacement transmissibility. As the damping ratio increases, the maximum value of the transmissibility decreases and it occurs at a lower frequency. However, large values of the damping ratio lead to higher transmissibility in the high-frequency region. Fig. 8 (b) shows the effect of varying the excitation amplitude $\hat{Z}_e$ on the displacement transmissibility. As the excitation amplitude increases, the maximum transmissibility increases and this peak occurs at a higher frequency. When the excitation amplitude exceeds a certain value, the maximum transmissibility of the 3rd-order HSLDS mount will be greater than that of the equivalent linear system and the frequency above which isolation is achieved (i.e. T_D<1) is also greater than that of the linear system.

To sum up the results of Fig. 8 (a) and (b), the vibration isolation performance of the 3rd-order HSLDS mount is more beneficial for small excitation amplitudes. When designing the 3rd-order HSLDS mount, increasing the damping ratio within an appropriate range is beneficial to extend the frequency range of vibration isolation and to reduce the resonance peak.

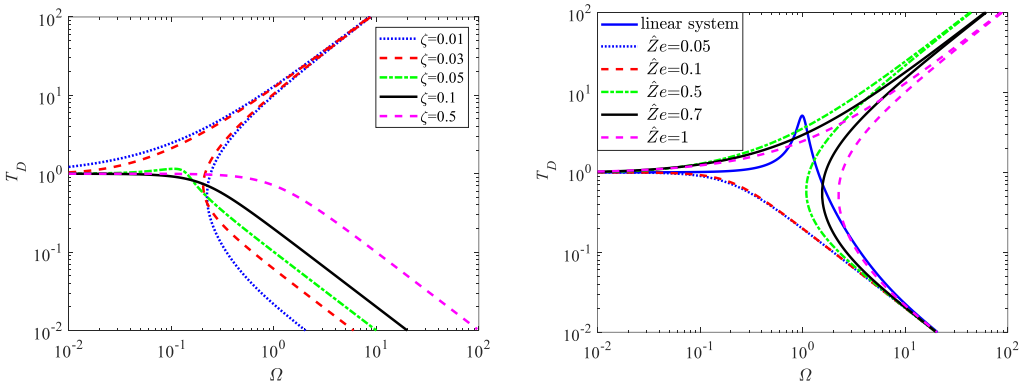

(a) (b)

Fig. 8. Displacement transmissibility of a third order system for (a) different damping ratio ζ (for $\hat{Z}_e$=0.1) and (b) different dimensionless excitation displacement $\hat{Z}_e$ (for ζ=0.1).

4 Prototype manufacturing and experimental study of a 3rd-order HSLDS mount

To demonstrate the applicability of the proposed design method for obtaining a certain HSLDS mount, a 3rd-order HSLDS mount has been designed and manufactured as a prototype for experimental research. The prototype is subjected to constant-frequency excitation experiments, and the transmission characteristics of the prototype are analyzed and compared with theoretical calculation results.

For a nonlinear system, if the stiffness at the equilibrium position is negative, the system will be unstable. Therefore, in the design and prototype manufacturing of the 3rd-order HSLDS mount, the target force curve adopts a 3rd-order HSLDS mount with a small additional linear stiffness, giving

$$f\left(x\right)=k_1x+k_3x^3 \tag{34}$$

where k_1=300N/m, k_3=3.5×10^5 N/m^3. This can prevent the system from having a negative stiffness at the equilibrium position due to manufacturing errors, and avoid instability. However, its value is not necessarily the same as the stiffness of the linear spring k_v. The target force-deflection curve and the corresponding stiffness characteristic are shown in Fig. 9(a) and (b), respectively. It can be seen that the stiffness has its minimum value at the equilibrium position, but this is greater than zero. The overall performance corresponds to a high static and low dynamic stiffness as intended.

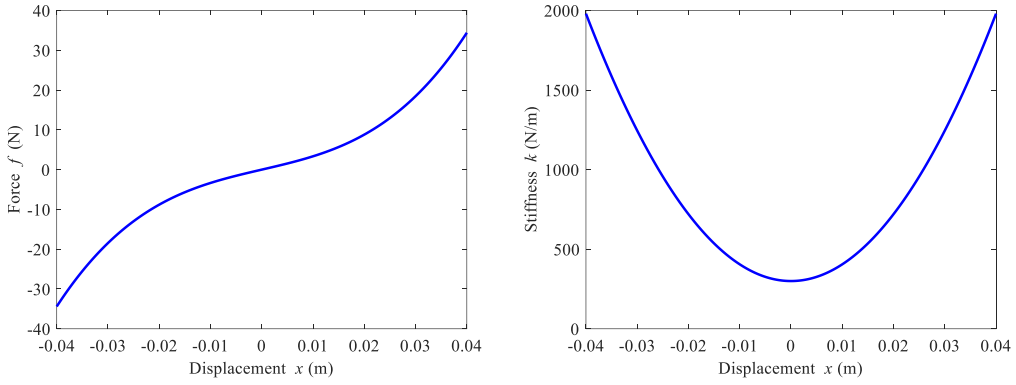

(a) (b)

Fig. 9. (a) Mechanical force-deflection characteristic curve of the prototype; (b) Stiffness characteristic curve of the prototype.

According to Eq. (4), the parameters shown in Tab. 1 are selected, and the guide curve corresponding to the target force curve can be obtained, as shown in Fig. 10. It can be seen from the figure that the entire guide curve is smooth and continuous, indicating that the design result is reasonable.

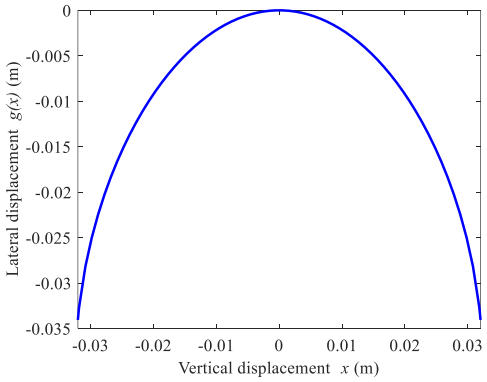

Fig. 10. Guide curve of the prototype.

Tab. 1 Parameters of the prototype

parameter	symbol	unit	value
Stiffness of vertical spring (each)	$k_v/2$	N/m	1010
Stiffness of lateral spring (each)	$k_h/2$	N/m	1010
Pre-compression length of lateral spring	$\triangle l$	mm	40
Mass of the isolated object	m	kg	6.15

The prototype has been designed and manufactured based on Fig. 1 and Fig. 10, and is shown in Fig. 11(a). The experimental prototype consists of a base, two lateral blocks, two lateral springs, two vertical springs, four guide posts, a vibration-isolated mass, two curved guide surfaces of height 80 mm, two rollers, and two height adjusters. The curved guide surfaces were manufactured by numerical computer-controlled milling and heat treatment. Other components of the rig were manufactured by wire-electrode cutting. The running surface of the roller is in line contact with the curved guide surface. The lateral spring-guide-roller mechanism is arranged symmetrically. The lateral blocks and the guide posts are connected by a linear bearing to reduce the frictional force due to the lateral movement in the guide post. Lateral springs, blocks, linear bearings, guide surfaces and rollers provide the negative stiffness in the vertical direction. Two vertical springs and guide posts are arranged in parallel (one behind the other in the photograph) so that the vibration-isolated mass only has freedom in the vertical direction. The vibration-isolated end is composed of a carrier plate and additional masses, and is connected to the vertical spring via the guide posts through a linear bearing. The height adjuster is used to ensure that the roller is in contact with the midpoint of the curved guide surface when the system is at the equilibrium position. A linear system is constructed by removing the lateral spring and the guide post, as shown in Fig. 11(b). Although the friction is not considered in the model design process, the friction force can be regarded as a part of the damping when the experimental results are compared with the theoretical results[29].

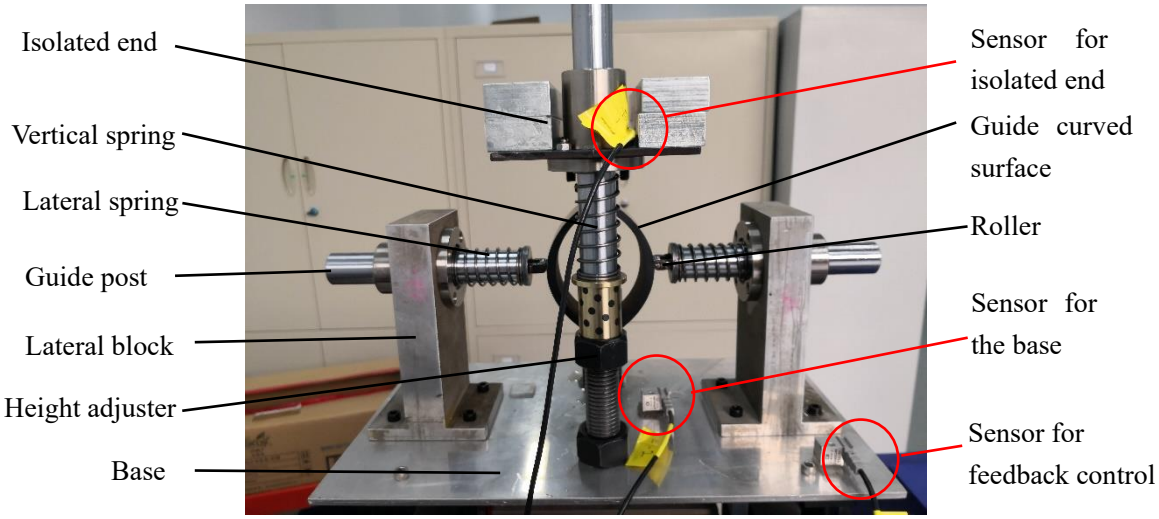

(a)

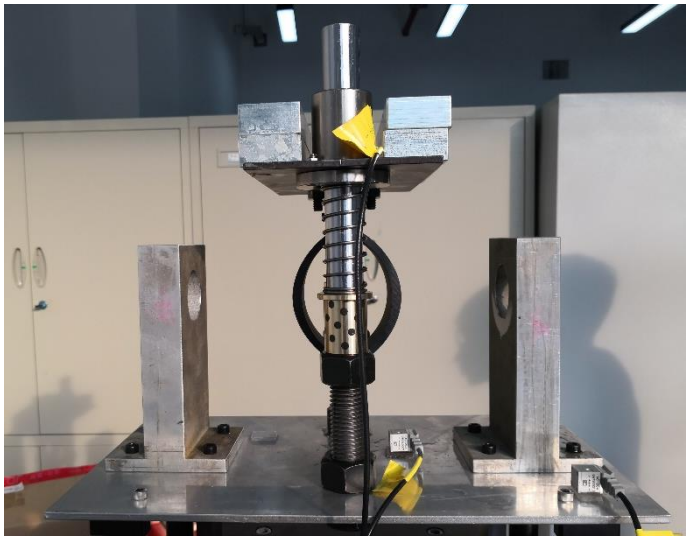

(b)

Fig. 11. (a) Prototype of the 3rd-order HSLDS mount; (b) Prototype of the linear system.

The static deflection of the 3rd-order HSLDS mount under the static load of the isolated mass mg is 50.5 mm (equivalent to a stiffness k_e = 1195 N/m), whereas for the linear system in Fig. 11(b) with a stiffness of k_v (2020 N/m) it is 29.9 mm. A linear system with a stiffness of k_1 (300 N/m) has a static deflection of 201 mm which is much greater than the 3rd-order HSLDS mount while they have the same dynamic stiffness at the equilibrium position.

The linear system was subjected to constant frequency excitation experiments in the range 0.7 to 10 Hz. By measuring the acceleration of the base and isolated mass, the acceleration transmissibility is calculated, as shown in Fig. 12. The theoretical results are included in the figure for comparison. The damping ratio in the theoretical result calculation is set to 0.042 to obtain good agreement with the measurement, and the remaining parameters are based on Tab. 1. It can be seen that the experimental results are in good agreement with the theoretical calculations. The peak of the transmissibility occurs at around 2.9 Hz, with a maximum value of about 12.

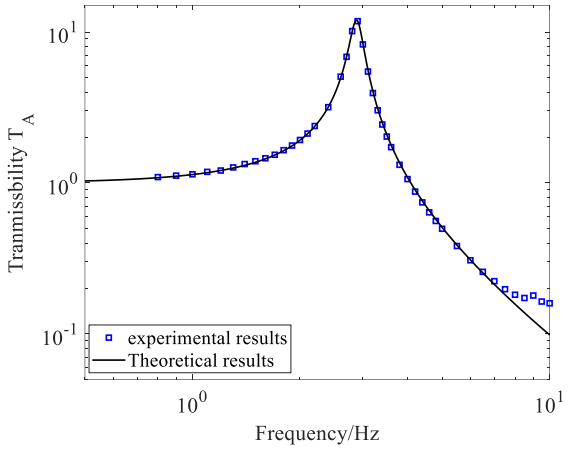

Fig. 12. Comparison between experiment and theoretical acceleration transmissibility of linear system.

The HSLDS mount was also subjected to constant-frequency excitation experiments in the range 0.7 to 10 Hz. The excitation amplitude was 12 mm, and the corresponding non-dimensional amplitude $\hat{Z}_e$ of the theoretical results is 0.4. The acceleration transmissibility is obtained as shown in Fig. 13. The theoretical results are included in the figure for comparison. In the theoretical calculation, the damping ratio is set to 0.12, which is higher than the value used for the linear system in Fig. 12. This is because the HSLDS mount have hysteresis due to the friction of the lateral spring-guide-roller mechanism, which acts to increase the damping of the system as is common in HSLDS systems[29]. It can be seen from the results that the experimental resonance peak of the HSLDS mount is 1.2 Hz, with a maximum transmissibility of 2.3. The theoretical calculation results are in good agreement with the experimental results, and the remaining differences are believed to be mainly caused by manufacturing errors and the influence of friction.

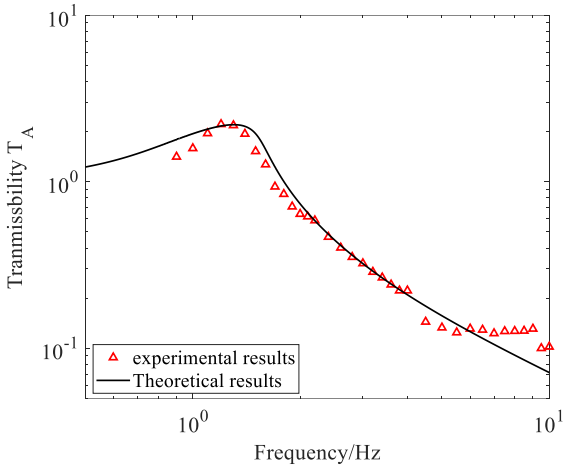

Fig. 13. Comparison between experiment and theoretical results of HSLDS mount.

Fig. 14 shows a comparison between the HSLDS mount and the linear system experimental results. In the figure, a theoretical result of the linear system is added based on the damping ratio of 0.12 for equivalence with the nonlinear system. It can be seen from the figure that the resonance frequency and the maximum transmissibility for the HSLDS mount are much lower than for the linear system, even allowing for the higher damping. Compared with the linear system, which shows vibration amplification below 4 Hz, the HSLDS mount only exhibits vibration amplification below 1.7 Hz. Summarizing Fig. 12 to Fig. 14, the HSLDS mount exhibits vibration isolation over a wider frequency range and has a lower resonance peak than the linear system.

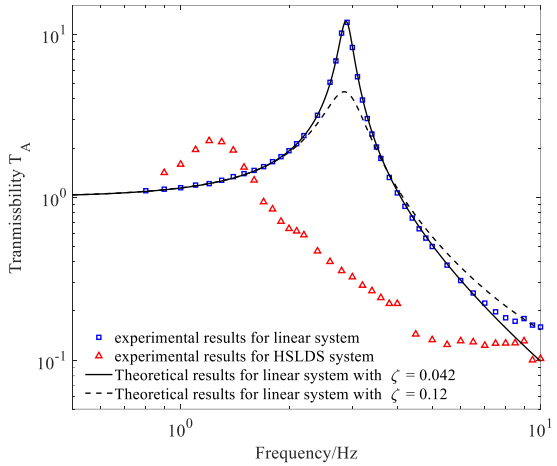

Fig. 14. Experimental results comparison between HSLDS mount and linear system.

5 Conclusions

In this paper, a design method for a HSLDS mount based on a target force curve is proposed, and *n*th-order HSLDS mounts are designed. Static analysis of the *n*th-order HSLDS mounts shows that, compared with lower order HSLDS mounts based on the same static stiffness, the higher-order HSLDS mount has a lower dynamic stiffness and larger stroke length near the equilibrium position.

The transmissibility under harmonic displacement excitation of the *n*th-order HSLDS mounts is calculated. The effects of nonlinear parameters, damping ratio and excitation amplitude on the system are analyzed. The results show that appropriately increasing the damping ratio is beneficial to improve the isolation performance of the HSLDS mounts. However, increasing the damping ratio by too much leads to a degradation of performance at high frequency.

Based on the 3rd-order HSLDS, an experimental prototype has been designed and manufactured, and the proposed design method is verified. The acceleration transmissibility of the prototype has been tested. The results show that the HSLDS mount has better vibration isolation performance. The HSLDS mount exhibits vibration isolation over a wider frequency range and has a lower resonance peak than the linear system. Its damping is increased to some extent by friction.

Further work would be required to provide suitable dimensioning of the concept presented here for practical applications. For example, for use as an isolation mount for a typical engine or similar piece of equipment, much larger stiffnesses than those achieved in the current prototype would be required including stiffer lateral springs. However, in terms of dimensioning, the height of the roller guides is mainly determined by the static deflection which in turn depends on the natural frequency (of the linear system) so the overall height is likely to be similar to that of the prototype. The HSLDS mount is only required in the vertical direction but to achieve suitable multi-dof isolation would require the inclusion of lateral (shear) mounts in series with the HSLDS mount.

Disclosure statement

No potential conflict of interest was reported by the authors.

Funding

This work is supported by National Natural Science Foundation of China: grant number 51805373.

References

[1] D. Gong, J.S. Zhou, W.J. Sun, et al. Method of multi-mode vibration control for the carbody of high-speed electric multiple unit trains. Journal of Sound and Vibration, 2017,409:94-111.

[2] G Papaioannou, A Voutsinas, D Koulocheris. Optimal design of passenger vehicle seat with the use of negative stiffness elements. Proceedings of the Institution of Mechanical Engineers, Part D: Journal of Automobile Engineering, 2020,234(2-3):610-629.

[3] K. Shiba, S. Mase, Y. Yabe, et al. Active/passive vibration control systems for tall buildings. Smart Materials & Structures, 1998,7(5):588-598.

[4] M. Vladimir, S. Vladimir. Optical Tables Vibration Isolation during Precision Measurements. Procedia Engineering, 2015,111:561-568.

[5] D. Gong, Y. Duan, K. Wang, et al. Modelling rubber dynamic stiffness for numerical predictions of the effects of temperature and speed on the vibration of a railway vehicle car body. Journal of Sound and Vibration, 2019,449:121-139.

[6] W.J. Sun, D. Thompson, J.S. Zhou. The influence of vehicle–track dynamic coupling on the fatigue failure of coil springs within the primary suspension of metro vehicles. Vehicle System Dynamics, 2019(12):1-17.

[7] E. Foo, R Goodall. Active suspension control of flexible-bodied railway vehicles using electro-hydraulic and electro-magnetic actuators. Control Engineering Practice, 2000, 8(5):507-518.

[8] International Organization for Standardization. Mechanical vibration and shock - Evaluation of human exposure to whole-body vibration - Part 1: General requirements. International Organization for Standardization. Standard No. ISO 2631-1. 1997.

[9] A.D. Shaw, S.A. Neild, D.J. Wagg. Dynamic analysis of high static low dynamic stiffness vibration isolation mounts. Journal of Sound and Vibration, 2013,332(6):1437-1455.

[10] P.A. Alabuzhev, L Gritchin, L Kim, et al. Vibration Protecting and Measuring Systems with Quasi-Zero Stiffness. 1989, New York.: Hemisphere Publishing.

[11] R.A. Ibrahim. Recent advances in nonlinear passive vibration isolators. Journal of Sound and Vibration, 2008,314(3-5):371-452.

[12] G Papaioannou, A Voutsinas, D Koulocheris, et al. Dynamic performance analysis of vehicle seats with embedded negative stiffness elements. Vehicle System Dynamics, 2019, 58(2):307-337.

[13] A. Carrella, M.J. Brennan, T.P. Waters. Optimization of a quasi-zero-stiffness isolator. Journal of Mechanical Science & Technology, 2007, 21(6):946.

[14] A. Carrella, M.J. Brennan, T.P. Waters. Static analysis of a passive vibration isolator with quasi-zero-stiffness characteristic. Journal of Sound and Vibration, 2007, 301(3-5):678-689.

[15] A. Carrella, M.J. Brennan, T.P. Waters, et al. Force and displacement transmissibility of a nonlinear isolator with high-static-low-dynamic-stiffness. International Journal of Mechanical Sciences, 2012,55(1):22-29.

[16] T.D. Le, K.K. Ahn. Experimental investigation of a vibration isolation system using negative

stiffness structure. International Journal of Mechanical Sciences, 2011, 70(5):99-112.

[17] T.D. Le, V.A.D. Nguyen. Low frequency vibration isolator with adjustable configurative parameter[J]. International Journal of Mechanical Sciences, 2017,134:224-233.

[18] X.T. Liu, X.C. Huang, H.X. Hua. On the characteristics of a quasi-zero stiffness isolator using Euler buckled beam as negative stiffness corrector. Journal of Sound and Vibration, 2013,332(14):3359-3376.

[19] X.C. Huang, X.T. Liu, J.Y. Sun, et al. Effect of the system imperfections on the dynamic response of a high-static-low-dynamic stiffness vibration isolator. Nonlinear Dynamics, 2014,76(2):1157-1167.

[20] X.C. Huang, X.T. Liu, J.Y. Sun, et al. Vibration isolation characteristics of a nonlinear isolator using Euler buckled beam as negative stiffness corrector: A theoretical and experimental study. Journal of Sound and Vibration, 2014,333(4):1132-1148.

[21] L.S. Meng, F. Liu. Design and analysis of a quasi-zero stiffness isolator using a slotted conical disk spring as negative stiffness structure. Journal of Vibroengineering, 2014,16(4):1769-1785.

[22] L.S. Meng, J.G. Sun, W.J. Wu. Theoretical Design and Characteristics Analysis of a Quasi-Zero Stiffness Isolator Using a Disk Spring as Negative Stiffness Element. Shock and Vibration, 2015:1-19.

[23] A. Valeev, A. Zotov, S. Kharisov. Designing of Compact Low Frequency Vibration Isolator with Quasi-Zero-Stiffness. Journal of Low frequency noise, Vibration and Active control, 2015,34(4):459-474.

[24] A. Valeev, A. Zotov, A. Tokarev. Study of Application of Vibration Isolators with Quasi-zero Stiffness for Reducing Dynamics Loads on the Foundation. Procedia Engineering, 2017,176:137-143.

[25] W.J. Wu, X.D. Chen, Y.H. Shan. Analysis and experiment of a vibration isolator using a novel magnetic spring with negative stiffness. Journal of Sound and Vibration, 2014, 333(13):2958-2970.

[26] A. Carrella, M.J. Brennan, T.P. Waters, et al. On the design of a high-static–low-dynamic stiffness isolator using linear mechanical springs and magnets. Journal of Sound and Vibration, 2008,315(3):712-720.

[27] G.X. Dong, X.N. Zhang, S.L. Xie, et al. Simulated and experimental studies on a high-static-low-dynamic stiffness isolator using magnetic negative stiffness spring. Mechanical Systems and Signal Processing, 2017,86:188-203.

[28] J.X. Zhou, X.L. Wang, D.L. Xu, et al. Nonlinear dynamic characteristics of a quasi-zero stiffness vibration isolator with cam–roller–spring mechanisms. Journal of Sound and Vibration. 2015, 346:53-69.

[29] M. Li, W. Cheng, R. Xie. Design and experiments of a quasi–zero-stiffness isolator with a noncircular cam-based negative-stiffness mechanism. Journal of Vibration and Control, 2020, 0(0):1-13.

[30] B.C. Wen. Engineering nonlinear vibration. Beijing: Science Press, 2007 (in Chinese)